Insulator Materials for Interface Passivation of Cu(In,Ga)Se_2 Thin Films

J. M. V. Cunha, P. A. Fernandes, A. Hultqvist, J. P. Teixeira, S. Bose, B. Vermang, S. Garud, D. Buldu, J. Gaspar, M. Edoff, J. P. Leitão, and P. M. P. Salomé

***Abstract*—In this work, metal–insulator–semiconductor structures were fabricated in order to study different types of insulators, namely, aluminum oxide (Al_2O_3), silicon nitride, and silicon oxide (SiO_x) to be used as passivation layers in Cu(In,Ga)Se_2 (CIGS) thin-film solar cells. The investigated stacks consisted of SLG/Mo/CIGS/insulator/Al. Raman scattering and photoluminescence measurements were done to verify the insulator deposition influence on the CIGS surface. In order to study the electrical properties of the CIGS–insulator interface, capacitance versus conductance and voltage (*C–G–V*) measurements were done to estimate the number and polarity of fixed insulator charges (Q_f). The density of interface defects (D_{it}) was estimated from capacitance versus conductance and frequency (*C–G–f*) measurements. This study evidences that the deposition of the insulators at high temperatures (300 °C) and the use of a sputtering technique cause surface modification on the CIGS surface. We found that, by varying the SiO_x deposition parameters, it is possible to have opposite charges inside the insulator, which would allow its use in different device architectures. The material with lower D_{it} values was Al_2O_3 when deposited by sputtering.**

***Index Terms*—Chemical passivation, Cu(In,Ga)Se_2 (CIGS), field-effect passivation, interface, passivation, solar cells, thin films.**

Manuscript received April 26, 2018; accepted May 31, 2018. Date of publication July 2, 2018; date of current version August 20, 2018. This work was supported by European Union's Horizon 2020 research and innovation programme ARCIGS-M project under Grant 720887. The work of J. M. V. Cunha and P. M. P. Salomé was supported by the Fundação para a Ciência e a Tecnologia (FCT) through the project IF/00133/2015. The work of J. P. Teixeira and J. P. Leitão was supported by the FCT through the project UID/CTM/50025/2013. The work of B. Vermang was supported by the European Research Council under the European Union's Horizon 2020 research and innovation programme under Grant 715027. *(Corresponding author: P. M. P. Salomé.)*

J. M. V. Cunha and J. Gaspar are with the International Iberian Nanotechnology Laboratory, Braga 4715-330, Portugal (e-mail: jose.cunha@inl.int; ao.gaspar@inl.int).

P. A. Fernandes is with the International Iberian Nanotechnology Laboratory, Braga 4715-330, Portugal, with CIETI, Departamento de Física, Instituto Superior de Engenharia do Porto, Instituto Politécnico do Porto, Porto 4200-072, Portugal, and also with I3N, Universidade de Aveiro, Aveiro 3810-193, Portugal (e-mail: paulo.fernandes@inl.int).

A. Hultqvist and M. Edoff are with the Ångström Laboratory, Solid State Electronics, Ångström Solar Center, Uppsala University, Uppsala SE-751 21, Sweden (e-mail: adam.hultqvist@angstrom.uu.se; marika.edoff@angstrom.uu.se).

J. P. Teixeira and J. P. Leitão are with I3N and Departamento de Física, Universidade de Aveiro, Aveiro 3810-193, Portugal (e-mail: jenniferpassos@ua.pt; joaquim.leitao@ua.pt).

S. Bose is with the International Iberian Nanotechnology Laboratory, Braga 4715-330, Portugal, and also with the Ångström Laboratory, Solid State Electronics, Ångström Solar Center, Uppsala University, Uppsala SE-751 21, Sweden (e-mail: sourav.bose@inl.int).

B. Vermang, S. Garud, and D. Buldu are with the University of Hasselt—Partner in Solliance, Diepenbeek 3590, Belgium, with IMEC—Partner in Solliance, Leuven 3001, Belgium, and also with IMOMEC—Partner in Solliance, Diepenbeek 3590, Belgium (e-mail: bart.vermang@imec.be; siddhartha.garud@helmholtz-berlin.de; Dilara.Gokcen.Buldu@imec.be).

P. M. P. Salomé is with the International Iberian Nanotechnology Laboratory, Braga 4715-330, Portugal, and also with the Departamento de Física, Universidade de Aveiro, Aveiro 3810-193, Portugal (e-mail: pedro.salome@inl.int).

Color versions of one or more of the figures in this paper are available online at http://ieeexplore.ieee.org.

Digital Object Identifier 10.1109/JPHOTOV.2018.2846674

I. Introduction

CURRENTLY, thin film solar cells based on Cu(In,Ga)Se_2 (CIGS) achieve an impressive world record of power conversion efficiency of 22.8% [1]. With material quality being the improvement of choice in the last decade for CIGS technology, in recent years a bigger focus on improving the interface quality has been made. At the front interface, a postdeposition treatment (PDT) that is constituted by the incorporation of alkali elements reduces the front interface recombination significantly [2]–[6]. While the exact mechanisms of the PDT process that lead to an increase in the electrical performance of the solar cells and its full effects are still being discussed, a study has shown that there is a formation of a nanopatterned layer [7]. At the rear interface, the introduction of a nanopatterned insulator layer that passivates the interface led to improvements in the power conversion efficiency of ultrathin CIGS solar cells of up to 2% [8]–[14]. In those cases, the point contacts assure electrical contact, while the passivation is made by an insulator made of aluminum oxide (Al_2O_3). The insulator materials have the potential to passivate the CIGS interface by lowering the number of interface defects, called chemical passivation, and by creating a built-in electrical field that repels carriers, called field-effect passivation [15], [16]. For the first studies, Al_2O_3 was the material of first choice as it is one of the best passivating materials in Si technology. For CIGS, an investigation of other oxide materials was performed as buffer layers in different solar cells configurations [17], [18] and as passivation layer [19] with different insulators than those studied in this work.

We report the study of several insulator materials, namely, Al_2O_3, silicon oxide (SiO_x), and silicon nitride (Si_3N_x), to be used as passivation materials in CIGS solar cells. For this purpose, we use an inverted metal–insulator–semiconductor (MIS) structure: SLG/Mo/CIGS/insulator/Al with the rear contact made of Mo. This architecture has the advantage that the CIGS growth is done in a similar way as for regular solar cells and the disadvantage that it does not allow for annealing of the insulator layers as it might cause CIGS surface modification,

2156-3381 © 2018 IEEE. Translations and content mining are permitted for academic research only. Personal use is also permitted, but republication/redistribution requires IEEE permission. See http://www.ieee.org/publications_standards/publications/rights/index.html for more information.

TABLE I
SAMPLE NAMING

Sample Name	*Sample Description*	*Structure*
Ref	CIGS reference sample	SLG/Mo/CIGS/CdS
$Al_2O_3 - S$	Al_2O_3 deposited by sputtering	SLG/Mo/CIGS/Al_2O_3
Si_3N_x	Si_3N_x deposited by PECVD at 150 ºC, HF	SLG/Mo/CIGS/Si_3N_x
$Al_2O_3 - ALD$	Al_2O_3 deposited by ALD	SLG/Mo/CIGS/Al_2O_3
SiO_x – 300 ºC	SiO_x deposited by PECVD at 300 ºC, HF	SLG/Mo/CIGS/SiO_x
SiO_x – 150 ºC, HF	SiO_x deposited by PECVD at 150 ºC, HF	SLG/Mo/CIGS/SiO_x
SiO_x – 150 ºC, LF	SiO_x deposited by PECVD at 150 ºC, LF	SLG/Mo/CIGS/SiO_x

LF means low-frequency deposition and HF means high-frequency deposition.

which can lead to interpretation problems. The annealing can change the insulator properties, namely, the polarity of the fixed insulator charges Q_f, and reduce the number of interface defects D_{it} [20]. Hence, our study is relevant for cases where no annealing of the insulators is made, which is the case of alternative CIGS architectures, such as superstrate [21] or novel ones. Besides applying MIS measurements for the determination of interface traps density and fixed insulator charges concentration and electrical polarity, we also focus our attention in understanding how the deposition conditions influence or cause CIGS surface modification.

II. EXPERIMENTAL

The main focus of this work is the study of the effects of several insulators, namely, Al_2O_3, Si_3N_x, and SiO_x on the CIGS interface properties. The samples started as soda-lime glass substrate, Mo rear contact (thickness of 350 nm), $Cu(In_{1-x}, Ga_x)Se_2$ as absorber layer (thickness of 2 μm), and CdS (thickness of 70 nm). The CdS was deposited on the top of CIGS to prevent air exposure of the CIGS during handling [22], [23]. The deposition of these layers was according to the Ångström solar cell baseline [24]. The samples names used henceforward are presented in Table I.

Before the insulator deposition, a 10% (w/w) HCl etch was done during 2 min to remove the CdS layer and to leave the CIGS surface pristine [25]. Subsequently, the samples were taken to the deposition tools in a matter of seconds to avoid CIGS air exposure.

The insulators were deposited with 50 nm and using different techniques.

1) Al_2O_3 by RF sputtering at 1500 W, Ar injection with a flow of 200 sccm and the deposition pressure of 5×10^{-3} mbar.
2) Si_3N_x by plasma enhanced chemical vapor deposition (PECVD) at 150 °C, high frequency (HF) of 13.56 MHz, plasma power of 30 W, and as precursor gases NH_3, SiH_{4-5}, and N_2.
3) SiO_x by PECVD at three different deposition conditions.
    a) 300 °C, HF, plasma power of 30 W, and as precursor gases N_2O, SiH_{4-5}, and N_2.

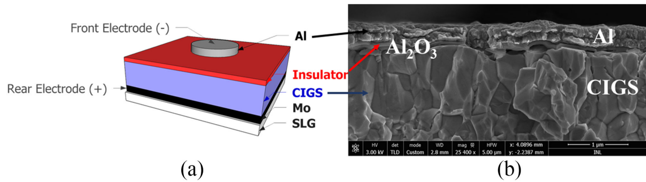

Fig. 1. (a) Scheme of the MIS structure: SLG/Mo/CIGS/insulator/Al. The molybdenum thickness is 350 nm, the CIGS is 2 μm, the insulator is 50 nm, and the aluminum layer is 400 nm (bilayer of 200 nm each). The image is not at scale. (b) SEM cross-section of sputtered Al_2O_3.

    b) 150 °C, HF, plasma power of 30 W, and as precursor gases N_2O, SiH_{4-5}, and N_2.
    c) 150 °C, low frequency (LF) of 380 kHz, plasma power of 60 W, and as precursor gases N_2O, SiH_{4-5}, and N_2.
4) Al_2O_3 by atomic layer deposition (ALD) at 200 °C, using as precursor gases trimethyl aluminum as the aluminum source and H_2O as the oxygen source.

To create the MIS structure, metal aluminum layer contacts were deposited by thermal evaporation, with a thickness of 400 nm. The final scheme of one MIS structure and a representative scanning electron microscopy (SEM) cross-section are depicted in Fig. 1. Each sample had 10 circular contacts with diameters of 1 mm, 5 contacts with diameters of 2 mm, and 6 contacts with diameters of 3 mm.

Raman spectroscopy was performed, using a confocal Raman microscope 300 R (WiTec) with green laser (excitation wavelength of 532 nm), 1 mW of power, and a Zeiss objective of 100× in the backscattering configuration. Photoluminescence (PL) was performed with a YAG, class 3B laser with a 15 kHz repetition rate and 1 ns pulse length with a beam spot of 3 mm and the excitation wavelength of 532 nm. An average illumination intensity of 1 mW was used. SEM cross-section was carried out, using a NovaNanoSEM 650 tool with an acceleration voltage of 3 kV.

C–G–f measurements were done using an Agilent E4890 A with 30 mV (V_{RMS}), 0 V_{bias} from 20 Hz to 1 MHz in frequency. *C–G–V* measurements were done in the same tool with 30 mV (V_{RMS}) and a frequency of 10 kHz. The ac electrical behavior of the MIS structures for the referred frequency range was modeled using ZSimpWin 3.50 software [26], where different equivalent circuits were tested. The software fits impedance data by varying resistance and capacitance values of a user-defined model circuit.

III. RESULTS AND DISCUSSION

A. CIGS Surface Modifications

One of the objectives of this study was to understand if the deposition of the insulators caused any surface modifications to the CIGS. In order to study surface morphological changes, Raman spectroscopy was performed and representative curves are shown in Fig. 2.

All the samples reveal the CIGS A_1 mode peak located at 172 cm^{-1} [27]. However, some of the samples, but not the reference one, show a shoulder in the low energy side of the referred

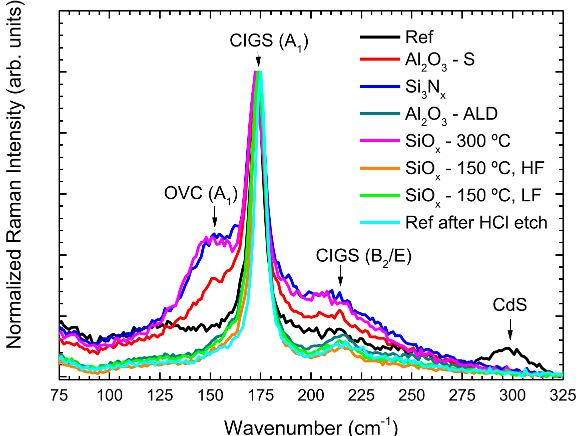

Fig. 2. Representative Raman spectra of all samples.

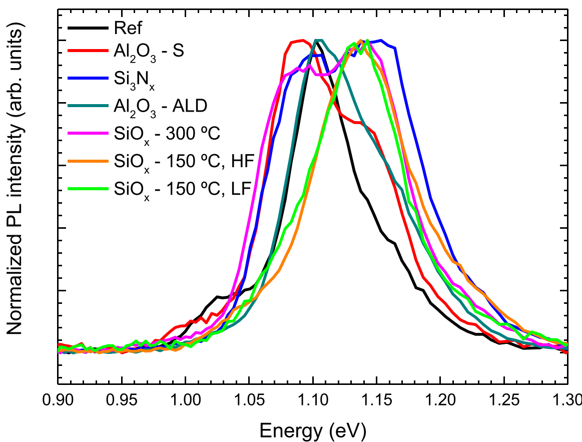

Fig. 3. Photoluminescence spectra of all samples.

CIGS peak. The shoulder, accordingly to the literature, is directly related to an order vacancy compound (OVC) [27], [28]. Al_2O_3-S, Si_3N_x, and SiO_x −300 °C samples show the OVC layer hinting to the fact that there was some surface modification during the insulator deposition, whereas Al_2O_3-ALD and both SiO_x deposited at 150 °C do not seem to cause modification to the CIGS surface, within the precision and accuracy limits of this equipment.

A probable reason for the OVC layer appearance is a CIGS surface modification [27], which could possibly be related to 1) the high energy sputtering method; 2) the high temperatures involved in the insulator deposition (300 °C); or 3) the HCl etch.

It is known that sputtering causes CIGS surface modification [29], [30], while the HCl etch should not cause any surface change [25]. To understand if the HCl etch caused CIGS surface modification, a Raman measurement was conducted before and after the HCl etching. The spectra of the reference sample and the etched sample show the same peaks; thus, it is safe to conclude that the HCl etch is not affecting the CIGS surface.

PL was used to qualitatively study the CIGS opto-electronic properties, as shown in Fig. 3. In general, more recombination channels result in a wider emission and in an increase in the number of emission peaks, which ultimately lead to a worse solar cell electrical performance [31]–[33]. Both SiO_x samples deposited at 150 °C and the Al_2O_3 sample deposited by ALD have only one narrow emission peak. The samples Al_2O_3-S, Si_3N_x, and SiO_x −300 °C show broad emissions. Consequently, a higher number of recombination channels should be present in the latter samples compared with the former ones. Besides having a narrow emission, both 150 °C SiO_x samples have a blue shift in the energy of its peak position as compared with the emission from the reference sample. Such blue shift can either represent a higher bandgap value (unlikely due to the same CIGS processing in these samples) or passivation of shallow defects [34], [35]. The Al_2O_3-S, Si_3N_x, and SiO_x −300 °C samples have an emission, which is characterized by two peaks. One of the peaks is located at the same energy as the one found in the reference sample and a second peak located at higher energetic positions. It is clear that the samples with the SiO_x deposited at 150 °C and the Al_2O_3 deposited by ALD have a lower number of recombination channels affecting their electronic structure, a behavior similar to the reference sample but with different values of full width at half-maximum. To summarize the PL data, the samples that show several peaks are likely to have several recombination channels, whereas the ones with the emission similar to the reference sample kept the same recombination mechanism.

A clear relation between Raman and PL measurements is observable: for Al_2O_3-S, Si_3N_x, and SiO_x −300 °C samples, CIGS-surface modifications are likely present. These samples involve deposition methods that are energetic and high-temperature processing; hence, there is enough energy to induce surface modifications. The other samples, presenting similar PL and Raman results with the reference sample, indicate no CIGS surface modification.

B. Interface Electrical Measurements

To study the insulators passivation effect, two parameters were estimated: fixed insulator charges Q_f and interface defects density D_{it}, in the CIGS–insulator interface.

The fixed insulator charges Q_f are estimated using the following equation [36]:

$$Q_f = \frac{C_{\text{in}}\,(\phi_{\text{MS}} - V_{\text{fb}})}{A \times q} \tag{1}$$

where A is the front metal contact area, q is the elementary charge, C_{in} is the insulator capacitance, and V_{fb} is the flat-band voltage. Φ_{MS} is the work function difference between metal and semiconductor and can be determined by [19], [36]

$$\phi_{\text{MS}} = \phi_M - \left(\chi + \frac{E_g}{2} + \frac{kT}{q}\ln\frac{N_a}{n_i}\right) \tag{2}$$

$$n_i = \sqrt{N_C N_V e^{\frac{-E_g}{kT}}} \tag{3}$$

where Φ_M is the aluminum work function (4.26 eV [37]), χ is the CIGS electron affinity (4.25 eV [38]), E_g is the CIGS bandgap (1.15 eV [24]), k is the Boltzmann constant, T is the temperature, N_a is the acceptor concentration (5×10^{15} cm^{-3}

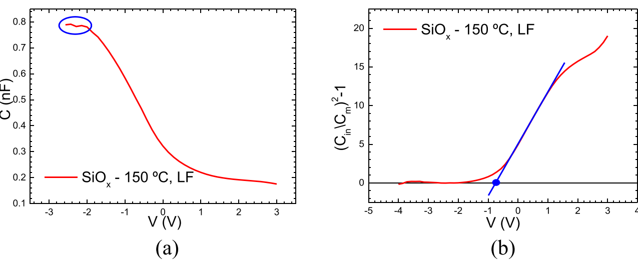

Fig. 4. Sample SiO_x-150 °C, LF. MIS with front contact of 1 mm. (a) Representative *C–V* curve. The blue circle corresponds to the region where the C_{in} value is extracted. (b) Representative V_{fb} extraction through the graphical method. The intercept of the fitted slope corresponds to -0.66 V.

TABLE II
Q_f VALUES TAKING INTO ACCOUNT THE AVERAGE C_{IN} AND V_{FB}. MIS WITH FRONT CONTACT DIAMETER OF 1 mm

	$Q_f \times 10^{11}$ (cm^{-2})
Al_2O_3 – S	+3.6
Si_3N_x	+3.2
Al_2O_3 – ALD	+4.1
SiO_x – 300 °C	+4.0
SiO_x – 150 °C, HF	+2.8
SiO_x – 150 °C, LF	-0.6

[19], [20]), n_i is the intrinsic carrier concentration, being calculated using (3) [19], N_c is the conduction-band density of states (7×10^{17} cm^{-3}), and N_v is the valence-band density of states (1.5×10^{19} cm^{-3}) [19], [39]. We note that when possible these values were experimentally calculated with CIGS fabricated under the same conditions as of this study and under these conditions, Φ_{MS} reaches a value of –0.97 V. However, some variability in the Al work function as well as in the CIGS affinity values is expected due to Ga content profile. We tested this hypothesis by changing Φ_M from 4.06 to 4.26 eV and χ from 4.25 to 4.5 eV and only minor changes to Φ_{MS} were observed. Despite this evidence, as Φ_{MS} is used to calculate Q_f, its absolute values should be seen with care, instead a comparison can be performed, as the CIGS and the aluminum are the same in all samples. In order to use (1), it is assumed that other insulator charges have a reduced effect on the Q_f measurements and that the interface traps play a negligible role [36], a common assumption in the literature but that has yet to be fully proved [40]–[42].

C–V–f measurements were done to determine the C_{in} and V_{fb} parameters necessary to the calculation of Q_f. C_{in} is the insulator capacitance value extracted from the strong accumulation regime in the *C–V* curve. Taking into account the CIGS p-type conductivity, the accumulation regime is found at negative bias. To get the values of flat-band voltage (V_{fb}), the graphical method [43] is used and the following equation is considered:

$$\left(\frac{C_{\text{in}}}{C_m}\right)^2 - 1 = 0 \quad (4)$$

where C_{in} is the insulator capacitance value, extracted in the *C–V* strong accumulation regime, and C_m is the measured capacitance.

A representative graph of the C_{in} and flat-band voltage (V_{fb}) extraction is shown in Fig. 4.

Averages and standard deviation for the Q_f values of the MIS structure with the front contact diameter of 1 mm are found in Table II. The large area MIS was not measured for reasons explained further in the text.

It is necessary to understand that the reference sample does not form an MIS structure; hence, it was not possible to calculate the electrical parameters such as Q_f and D_{it}. Considering Table II, it was expected that the same material had the same polarity of the fixed charges, as it is shown for the Al_2O_3 samples. However, an interesting observation is that for SiO_x-150 °C by changing frequency, in the deposition, it is possible to invert the polarity of the fixed insulator charges. Moreover, the insulator with positive charges (SiO_x-150 °C, HF) can be used in solar cells architectures that prefer field-effect passivation for holes, while the insulator with negative charges is more appropriate for rear passivation of current CIGS solar cells architectures as their field-effect passivation should repeal electrons.

This preliminary analysis shows that the interface Q_f values are not intrinsic to each insulator and that its concentration can be modified with growth properties.

The studied MIS structures had diameters of 1, 2, and 3 mm. However, during some of the *C–V* measurements, untypical behaviors appeared for the 2 and 3 mm MIS devices. Untypical behaviors of the large contact area devices observed were caused by a resistive behavior instead of a single capacitive one. An ideal MIS structure can be characterized by the equivalent circuit presented in Fig. 5(a). In this circuit, C_p and G_p correspond to the frequency-dependent capacitance and the frequency-dependent conductance, respectively, associated with the interface-traps, whereas C_{in} is the capacitance created by the insulator [36], [44], [45]. In such ideal equivalent circuit, shunt conduction in the insulator is neglected, which can be a problem for leaking current in the capacitor. In that case, a more realistic equivalent circuit would be the one presented in Fig. 5(b), where G_s is now present. However, for the case in Fig. 5(b), there are still no established models for parameters extraction with these circuit conditions. To identify if our devices were being heavily affected by insulator shunts, the frequency-dependent impedance behavior was measured. Afterward, these data were fitted to the equivalent circuit in Fig. 5(b), and values of G_s were extracted using the software ZSimpWin, which provides us with values of each electric component present in the circuit. Such procedure is needed as the measurement device considers the equivalent circuit shown in Fig. 5(c) and the measured values are C_m and G_m.

The extracted values for series conductance G_s are shown in Table III. As hinted from the *C–V* measurements, the series conductance values increase with the increasing contact diameter. These results indicate that while for small font contact

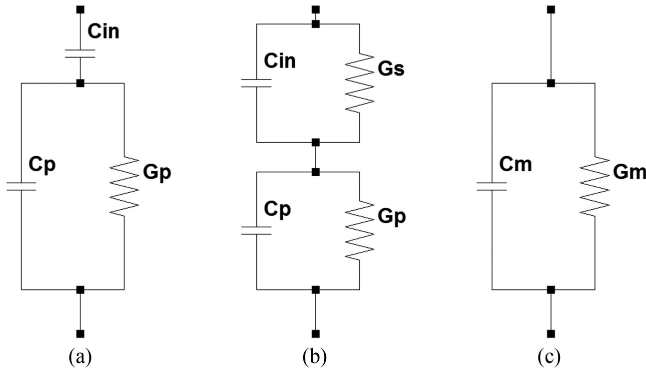

Fig. 5. Equivalent MIS circuits for conductance measurements. (a) Including interface-trap effect [45]. (b) Same circuit of (a), considering a possible series conductance. (c) Device's measured circuit.

TABLE III
AVERAGE AND STANDARD DEVIATION OF SERIES CONDUCTANCE FOR DIFFERENT TOP CONTACT DIAMETERS

G_s (nS)	1 mm	2 mm	3 mm
Si_3N_x	20.9 ± 6.70	92.9 ± 26.2	(1.34 ± 0.28) x10^5
Al_2O_3 - ALD	2.77 ± 1.25	14.7 ± 12.6	-
SiO_x - 300 °C	11.3 ± 1.70	38.0 ± 5.00	146 ± 49.0
SiO_x - 150 °C, HF	25.4 ± 17.1	302 ± 201	1.00 x10^3
SiO_x - 150 °C, LF	17.2 ± 6.70	103 ± 11.0	302 ± 54.0

diameters the electrical measurements are consistent with the circuit represented in Fig. 5(a), this is not the case for the other diameters. The results for 3 mm of the Al_2O_3-ALD sample are not represented since the error values were too high, showing the need for even more complex equivalent circuits. Henceforth, only results for 1 mm MIS structures will be shown.

Another important parameter for interface passivation is the density of interface defects (D_{it}). For a comparison between the D_{it} values of each sample, the conductance method, introduced by Nicollian and Brews [44], was used. This method does not assume the leakage current through the insulator; thus, G_s does not appear in (5). The value G_p for the ideal MIS structure presented in Fig. 5(a) is given by [44], [45]

$$\left(\frac{G_p}{\omega}\right) = \frac{\omega G_m C_{\text{in}}^2}{G_m^2 + \omega^2 (C_{\text{in}} - C_m)^2} \quad (5)$$

where ω is the angular frequency, G_m and C_m are the measured conductance and capacitance, respectively, and C_{in} is the capacitance of a *C–V* curve measured in the strong accumulation regime [36], [44], [45]. Plotting (G_{p}/ω) against frequency *f* will yield a maximum in the energy loss mechanism [20], [45], as shown in a representative plot in Fig. 6.

The relation is given by [20], [36]

$$D_{\text{it}} = \left(\frac{2.5}{A \times q}\right)\left(\frac{G_p}{\omega}\right)_{\text{max}} \quad (6)$$

The extracted D_{it} values are summarized in Table IV. Surprisingly most of the samples show D_{it} values within the same order of magnitude, being the notable exception the sputtered Al_2O_3

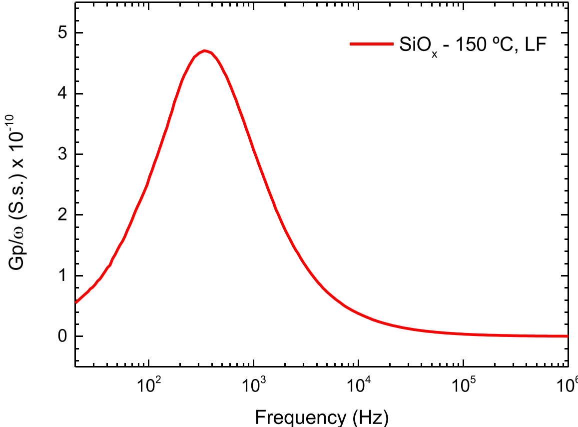

Fig. 6. Representative (G_p/ω) against *f* curve of sample SiO_x-150 °C, LF. MIS with 1 mm.

TABLE IV
D_{IT} AVERAGE AND STANDARD DEVIATION VALUES OF MIS WITH THE DIAMETER OF 1 MM FOR EACH SAMPLE

	D_{it} ×10^{12} (eV^{-1}cm^{-2})
Al_2O_3 – S	0.8 ± 0.03
Si_3N_x	1.6 ± 1.0
Al_2O_3 – ALD	3.8 ± 1.4
SiO_x – 300 °C	3.1 ± 1.9
SiO_x – 150 °C, HF	5.7 ± 3.2
SiO_x – 150 °C, LF	0.9 ± 0.09

sample. This is a remarkable result as the sputtering of Al_2O_3 was shown previously to cause some surface modifications and one would expect a higher number of electrical traps compared with samples with reduced surface modifications. While we cannot discard modifications to the composition of the Al_2O_3 layer itself in the sputtering deposition, the biggest difference compared with the ALD sample is the presence of an OVC layer. In the literature, there are several hypotheses that the OVC layer improves the interface, like for instance due to a similar crystal structure and better band alignment [46]–[49]. Such improvement might be an explanation for the superior results achieved with the sputtered Al_2O_3 sample in comparison with the ALD Al_2O_3.

There are models to represent the (G_{p}/ω) data, namely, the single-level defects and continuous distributions of defects [36]. Fittings were done to our data, and the most suitable model in our case is the single-level defect. Moreover, it was possible to extract D_{it} values through the fittings, and the values were found to be lower than the ones calculated using (6); however, they followed exactly the same trend of the calculated values in the present paper. Such fact is a good indication that comparisons of the D_{it} values between samples are possible to be made. However, the presented values should not be considered absolute val-

ues as a more detailed analysis has to be performed in the future to understand what is the most accurate D_{it} extraction technique.

IV. Conclusion

In this work, we studied the influence of depositing several insulator materials on CIGS with the objective of being used as interface passivation layers. We focused our attention in two different types of effects: 1) identification of CIGS surface modifications during the deposition of the insulator; and 2) comparison of the electrical effect on the interface between CIGS and passivation layer. For surface modification we identified two trends: 1) the appearance of an OVC layer; and 2) unchanged samples. It was shown that the deposition of the insulator with either sputtering or high temperatures (300 °C) causes the appearance of an OVC layer at the CIGS surface. Such fact was probed by Raman, and also seen in PL measurements by increased number of recombination channels.

With regard to the electrical measurements of the MIS structures, we determined that large areas lead to increased shunting between the Al contact and the Mo, which had to be dealt with by using sufficiently small values of the front contact area.

For the fixed insulator charges, the values were found to be similar between each other with the same positive electrical polarity; however, for the SiO_x deposited by LF, the values were found to be negative. The opposite polarity of the fixed charges means that the same insulator can be used for different passivation roles. On the subject of density of interface defects, the insulator with lower D_{it} values compared with the others insulators was Al_2O_3 deposited by sputtering. We note that a complete study of these effects has to be a continuous effort and more information, like defect energy and defect cross section, is needed in order to fully understand the effects of interface defects on the CIGS performance.

References

[1] R. Kamada *et al.*, "New world record Cu(In,Ga)(Se,S)$_2$ thin film solar cell efficiency beyond 22%," in *Proc. IEEE 43rd Photovolt. Spec. Conf.*, 2016, pp. 1287–1291.

[2] G. Sozzi *et al.*, "Impact of front-side point contact/passivation geometry on thin-film solar cell performance," *Sol. Energy Mater. Sol. Cells*, vol. 165, pp. 94–102, 2017.

[3] D. Abou-Ras *et al.*, "Innovation highway: Breakthrough milestones and key developments in chalcopyrite photovoltaics from a retrospective viewpoint," *Thin Solid Films*, vol. 633, pp. 2–12, 2017.

[4] A. Chirilă *et al.*, "Potassium-induced surface modification of Cu(In,Ga)Se$_2$ thin films for high-efficiency solar cells," *Nature Mater.*, vol. 12, pp. 1107–1111, Nov. 2013.

[5] P. Jackson *et al.*, "Effects of heavy alkali elements in Cu(In,Ga)Se$_2$ solar cells with efficiencies up to 22.6%," *Phys. Status Solidi, Rapid Res. Lett.*, vol. 10, no. 8, pp. 583–586, 2016.

[6] P. M. P. Salomé, H. Rodriguez-Alvarez, and S. Sadewasser, "Incorporation of alkali metals in chalcogenide solar cells," *Sol. Energy Mater. Sol. Cells*, vol. 143, pp. 9–20, 2015.

[7] E. Avancini *et al.*, "Effects of rubidium fluoride and potassium fluoride postdeposition treatments on Cu(In,Ga)Se$_2$ thin films and solar cell performance," *Chem. Mater.*, vol. 29, no. 22, pp. 9695–9704, Nov.2017.

[8] B. Vermang, V. Fjällström, J. Pettersson, P. Salomé, and M. Edoff, "Development of rear surface passivated Cu(In,Ga)Se$_2$ thin film solar cells with nano-sized local rear point contacts," *Sol. Energy Mater. Sol. Cells*, vol. 117, pp. 505–511, 2013.

[9] B. Vermang *et al.*, "Employing Si solar cell technology to increase efficiency of ultra-thin Cu(In,Ga)Se$_2$ solar cells," *Prog. Photovolt. Res. Appl.*, vol. 22, no. 10, pp. 1023–1029, 2014.

[10] B. Vermang, V. Fjallstrom, X. Gao, and M. Edoff, "Improved rear surface passivation of Cu(In,Ga)Se$_2$ solar cells: A combination of an Al_2O_3 rear surface passivation layer and nanosized local rear point contacts," *IEEE J. Photovolt.*, vol. 4, no. 1, pp. 486–492, Jan. 2014.

[11] P. M. P. Salomé *et al.*, "Passivation of interfaces in thin film solar cells: Understanding the effects of a nanostructured rear point contact layer," *Adv. Mater. Interfaces*, vol. 5, 2018, Art. no. 1701101.

[12] M. Schmid, P. Manley, A. Ott, M. Song, and G. Yin, "Nanoparticles for light management in ultrathin chalcopyrite solar cells," *J. Mater. Res.*, vol. 31, pp. 3273–3289, Nov. 2016.

[13] G. Yin *et al.*, "Well-controlled dielectric nanomeshes by colloidal nanosphere lithography for optoelectronic enhancement of ultrathin Cu(In,Ga)Se$_2$ Solar Cells," *ACS Appl. Mater. Interfaces*, vol. 8, no. 46, pp. 31646–31652, Nov. 2016.

[14] G. Yin *et al.*, "Optoelectronic enhancement of ultrathin $CuIn_{1-x}Ga_xSe_2$ solar cells by nanophotonic contacts," *Adv. Opt. Mater.*, vol. 5, no. 5, 2017, Art. no. 1600637.

[15] B. Vermang *et al.*, "Introduction of Si PERC rear contacting design to boost efficiency of Cu(In,Ga)Se$_2$ solar cells," *IEEE J. Photovolt.*, vol. 4, no. 6, pp. 1644–1649, Nov. 2014.

[16] M. A. Green, "The passivated emitter and rear cell (PERC): From conception to mass production," *Sol. Energy Mater. Sol. Cells*, vol. 143, pp. 190–197, 2015.

[17] T. Koida, Y. Kamikawa-Shimizu, A. Yamada, H. Shibata, and S. Niki, "Cu(In,Ga)Se$_2$ solar cells with amorphous oxide semiconducting buffer layers," *IEEE J. Photovolt.*, vol. 5, no. 3, pp. 956–961, May 2015.

[18] M. D. Heinemann *et al.*, "Amorphous oxides as electron transport layers in Cu(In,Ga)Se$_2$ superstrate devices," *Phys. Status Solidi*, vol. 214, no. 5, 2017, Art. no. 1600870.

[19] S. Garud *et al.*, "Surface passivation of CIGS solar cells using gallium oxide," *Phys. Status Solidi*, vol. 215, no. 7, Apr. 2018, Art. no. 1700826.

[20] R. Kotipalli *et al.*, "Investigating the electronic properties of Al_2O_3/Cu(In,Ga)Se$_2$ interface," *AIP Adv.*, vol. 5, no. 10, Oct. 2015, Art. no. 107101.

[21] M. Terheggen *et al.*, "Ga_2O_3 segregation in Cu(In, Ga)Se$_2$/ZnO superstrate solar cells and its impact on their photovoltaic properties," *Thin Solid Films*, vols. 403–404, pp. 212–215, 2002.

[22] R. Naciri *et al.*, "The role of CdS buffer layer in $CuInS_2$ based thin film solar cells," *Phys. Chem. News*, vol. 46, pp. 21–25, Jan. 2009.

[23] D. Regesch *et al.*, "Degradation and passivation of $CuInSe_2$," *Appl. Phys. Lett.*, vol. 101, no. 11, Sep. 2012, Art. no. 112108.

[24] J. Lindahl *et al.*, "Inline Cu(In,Ga)Se$_2$ Co-evaporation for high-efficiency solar cells and modules," *IEEE J. Photovolt.*, vol. 3, no. 3, pp. 1100–1105, Jul. 2013.

[25] D. Liao and A. Rockett, "Cd doping at the $CuInSe_2$/CdS heterojunction," *J. Appl. Phys.*, vol. 93, no. 11, pp. 9380–9382, May 2003.

[26] B. Yeum, "Electrochemical impedance spectroscopy: Data analysis software," Echem Software, Ann Arbor, MI, USA, 2001.

[27] J. Bi *et al.*, "Pulse electro-deposition of copper on molybdenum for Cu(In,Ga)Se$_2$ and $Cu_2ZnSnSe_4$ solar cell applications," *J. Power Sources*, vol. 326, pp. 211–219, 2016.

[28] J. Wang, J. Zhu, and Y. X. He, "The influence of different locations of sputter guns on the morphological and structural properties of Cu–In–Ga precursors and Cu(In,Ga)Se$_2$ thin films," *Appl. Surf. Sci.*, vol. 288, pp. 109–114, 2014.

[29] M. Sugiyama, H. Sakakura, S.-W. Chang, and M. Itagaki, "Investigation of sputtering damage around pn interfaces of Cu(In,Ga)Se$_2$ solar cells by impedance spectroscopy," *Electrochim. Acta*, vol. 131, pp. 236–239, 2014.

[30] X. He *et al.*, "Intermixing and formation of Cu-rich secondary phases at sputtered CdS/$CuInGaSe_2$ heterojunctions," *IEEE J. Photovolt.*, vol. 6, no. 5, pp. 1308–1315, Sep. 2016.

[31] P. M. P. Salomé *et al.*, "Influence of CdS and ZnSnO buffer layers on the photoluminescence of Cu(In,Ga)Se$_2$ thin films," *IEEE J. Photovolt.*, vol. 7, no. 2, pp. 670–675, Mar. 2017.

[32] J. P. Teixeira *et al.*, "Radiative transitions in highly doped and compensated chalcopyrites and kesterites: The case of Cu_2ZnSnS_4," *Phys. Rev. B*, vol. 90, no. 23, Dec. 2014, Art. no. 235202.

[33] T. Gokmen, O. Gunawan, T. K. Todorov, and D. B. Mitzi, "Band tailing and efficiency limitation in kesterite solar cells," *Appl. Phys. Lett.*, vol. 103, no. 10, Sep. 2013, Art. no. 103506.
[34] M. V. Yakushev *et al.*, "Effects of D+ implantation of CIGS thin films through a CdS layer," *Thin Solid Films*, vol. 387, no. 1, pp. 201–204, 2001.
[35] R. Bacewicz, P. Zuk, and R. Trykozko, "Photoluminescence study of ZnO/CdS/$Cu(In,Ga)Se_2$ solar cells," *Opto-Electron. Rev.*, vol. 11, no. 4, pp. 277–280, Dec. 2003.
[36] D. K. Schroder, *Semiconductor Material and Device Characterization*, 3rd ed. Hoboken, NJ, USA: Wiley, 2005.
[37] W. M. Haynes, *CRC Handbook of Chemistry and Physics*, 96th ed. Boca Raton, FL, USA: CRC Press, 2015.
[38] C. Frisk *et al.*, "Optimizing Ga-profiles for highly efficient $Cu(In, Ga)Se_2$ thin film solar cells in simple and complex defect models," *J. Phys. D, Appl. Phys.*, vol. 47, no. 48, Dec. 2014, Art. no. 485104.
[39] A. Bercegol *et al.*, "Point contacts at the copper-indium-gallium-selenide interface—A theoretical outlook," *J. Appl. Phys.*, vol. 119, no. 15, Apr. 2016, Art. no. 155304.
[40] G. Dingemans, N. M. Terlinden, M. A. Verheijen, M. C. M. van de Sanden, and W. M. M. Kessels, "Controlling the fixed charge and passivation properties of Si(100)/Al_2O_3 interfaces using ultrathin SiO_2 interlayers synthesized by atomic layer deposition," *J. Appl. Phys.*, vol. 110, no. 9, Nov. 2011, Art. no. 93715.
[41] X. Tang *et al.*, "Room temperature atomic layer deposition of Al2O3 and replication of butterfly wings for photovoltaic application," *J. Vac. Sci. Technol. A*, vol. 30, 2011, Art. no. 01A146.
[42] R. Kotipalli *et al.*, "Passivation effects of atomic-layer-deposited aluminum oxide," *EPJ Photovolt.*, vol. 4, Sep. 2013, Art. no. 45107.
[43] K. Piskorski and H. M. Przewlocki, "The methods to determine flat-band voltage V_{FB} in semiconductor of a MOS structure," in *Proc. 33rd Int. Convention MIPRO*, 2010, pp. 37–42.
[44] E. H. Nicollian and J. R. Brews, *MOS (Metal Oxide Semiconductor) Physics and Technology*. Hoboken, NJ, USA: Wiley, 1982.
[45] S. M. Sze and K. K. Ng, *Physics of Semiconductor Devices*. Hoboken, NJ, USA: Wiley, 2006.
[46] T. Dullweber, G. H. Anna, U. Rau, and H. W. Schock, "A new approach to high-efficiency solar cells by band gap grading in $Cu(In,Ga)Se_2$ chalcopyrite semiconductors," *Sol. Energy Mater. Sol. Cells*, vol. 67, no. 1, pp. 145–150, 2001.
[47] T. Minemoto *et al.*, "Theoretical analysis of the effect of conduction band offset of window/CIS layers on performance of CIS solar cells using device simulation," *Sol. Energy Mater. Sol. Cells*, vol. 67, no. 1, pp. 83–88, 2001.
[48] A. Rockett *et al.*, "Near-surface defect distributions in $Cu(In,Ga)Se_2$," *Thin Solid Films*, vol. 431, pp. 301–306, May 2003.
[49] C.-H. Chung, K.-H. Hong, D.-K. Lee, J. H. Yun, and Y. Yang, "Ordered vacancy compound formation by controlling element redistribution in molecular-level precursor solution processed $CuInSe_2$ thin films," *Chem. Mater.*, vol. 27, no. 21, pp. 7244–7247, Nov. 2015.

Authors' photographs and biographies not available at the time of publication.